



A deep learning based lightning location system

Shayan Dodge ^a, Martino Nicora ^b*^{*}, Sami Barmada ^a, Massimo Brignone ^b, Renato Procopio ^b, Mauro Tucci ^a

^a Department of Energy, Systems, Territory and Construction Engineering (DESTEC), University of Pisa, Pisa, I- 56126, Italy

^b Department of Naval, Electronic, Electrical and Telecommunication Engineering (DITEN), University of Genoa, Genoa, I-16145, Italy

ARTICLE INFO

Keywords:

Deep learning
Artificial neural networks
Lightning location
Lightning current measurement
Lightning-induced voltage
Transmission lines

ABSTRACT

The paper presents a new approach for lightning location and peak current estimation based on Deep Learning (DL) algorithms. The basic idea is to use the time domain waveforms of the overvoltages induced by lightning strikes on transmission or distribution lines as features to regress both the location and the channel base current peak of a lightning event. Starting from previous research findings, the performance of the method have been further increased by proposing three different DL models, working either in the frequency or in the time domain. All models are trained with data simulated with the Lightning Power Electromagnetic Simulator for Transient Overvoltages (LIGHT-PESTO). The performances of the methods are first assessed on the same test case as the one presented in a previously published paper to show their increased effectiveness. Then, the best performing model among the three is tested on a more realistic network to show that, even in presence of much more complex systems, its performances are not reduced.

1. Introduction

The risk associated with lightning affects several aspects. Direct and indirect lightning strikes represent critical issues for power and telecommunication systems, leading to common disturbances, service interruptions and faults. On the other hand, lightning events can cause injuries on humans and animals as well as severe damages on buildings and structures, especially those with considerable height and/or located in isolated regions (e.g., wind turbines).

Lightning activity is monitored to infer valuable information aimed at risk mitigation. In particular, at least two quantities are included in all lightning risk assessments: the distance between the discharge source and the object to protect, and the magnitude related to the lightning event. Thus, from Cloud-to-Ground (CG) lightning location data it is possible to evaluate the ground stroke density and the ground flash density for specific regions, whereas a good indicator of the magnitude is the peak current (i.e., the maximum of the current discharge waveform at the base of the lightning channel [1]). An example consists in the evaluation of the lightning performance of transmission and distribution lines (e.g., [2–5]), which is the evaluation of the expected direct and indirect flash-overs per year experienced by the considered power system [6].

However, lightning location and peak current data are useful also for meteorology applications. Since the significant correlation between lightning and extreme weather events has been assessed [7], lightning

forecasting and nowcasting tools [8–10] the goal of preventing their effects.

Currently, the localization of CG lightning strikes primarily relies on Lightning Location Systems (LLS). These systems are networks of sensors spaced between 50 and 400 km and detecting the electromagnetic signals associated with CG discharges from the Very Low Frequency (VLF) to the Low Frequency (LF) range. In this type of systems, location techniques like magnetic direction finding, time-of-arrival, and combined modes are implemented to estimate the coordinates of the lightning strike.

Considering the Italian LLS (which is integrated into the European Cooperation for Lightning Detection, EUCLID), a 250-m median value for the CG lightning Location Accuracy (LA) has been reported. Indeed, such a parameter is not uniform in all the LLS detection area due to sensors distance and advance.

Moreover, LLS perform a peak current estimation applying a simple linear model inputted with the peak E-field and the estimated distance, for the entire range of current amplitudes up to over 100 kA (including positive return strokes) [11]. Such a conversion, which is based on the far field approximation, is affected by some open issues: (i) during the last decade, LLS detection efficiency has been significantly improved, with the drawback of having incremented classification errors (especially consisting in cloud discharges labeled as positive CG strokes with low amplitude) which can produce bias on the peak current

* Corresponding author.

E-mail address: martino.nicora@edu.unige.it (M. Nicora).

distributions provided by LLS, and (ii) the process of converting field measurements to estimate the current peak have so far been validated only for subsequent negative return strokes with current amplitudes less than 40 kA [12] (up to 60 kA for the U.S.A. National Lightning Detection Network [13]), utilizing data from rocket-triggered lightning experiments and measurements from instrumented towers. So, this validation does not necessarily extend to negative and positive first strokes, as well as positive subsequent strokes [14].

On the other hand, current measurements directly taken at instrumented towers [15–20] are limited to a very low numbers of events recorded during a selected time window and concerning only the location where such towers are installed. Nevertheless, due to the high reliability of such systems, the waveform parameters of the lightning current reported by Berger and coworkers [15] remain the present-day standard.

In this framework, alternative systems based on Machine Learning (ML) techniques have been proposed recently with the purpose of performing CG lightning location [21,22] and peak current estimation [22] starting from measurements of the voltage waveforms induced by lightning strikes on overhead transmission and distribution lines.

This research line is supported by the possibility, in principle, of developing a final system capable of achieving two main objectives: (i) to perform an accurate lightning location with a precision at least of the same order of LLS and with the advantage of not requiring ad hoc devices, and (ii) to provide a more precise estimation of peak current compared to LLS, that should be more up-to-date and cover a much wider domain than direct tower measurements.

The authors of [21] presented a first development of this concept. They proposed a ML algorithm regressing the lightning location coordinates and trained with voltage waveforms simulated using the Rusck's approximate formula [23], that applies only to single-phase transmission lines of infinite length, with no losses and under the perfectly conducting ground assumptions. Moreover, the current waveform at the base of the lightning channel has been assumed as a step source. Beyond the strong approximations, the results of [21] in terms of localization error have somehow justified the goodness of the approach.

Successively, a more accurate model for the lightning discharge, electromagnetic fields and induced voltage, and the lossy ground case has been considered in [22] by means of the Lightning Power Electromagnetic Simulator for Transient Overvoltages (LIGHT-PESTO) [24]. The lightning localization and current peak estimation has been performed with a sequence of two shallow feed-forward Neural Networks (NN) trained with the harmonic content of the voltage waveforms processed with a Principal Components Analysis (PCA). Test performed on a 10-km straight single line, matched at both extremities laying over a lossy ground have revealed an average location error of 290 m, i.e., comparable to the state of the art of LLS in Italy. Moreover, this algorithm provided an estimation of the peak current with a 12.5% accuracy and a significant correlation with the predicted location (81%).

More recently, an attempt to extend to subsequent return stroke localization the approach of [22] has been proposed in [25], and a single-sensor ML-based lightning localization system as been presented in [26] using data simulated on a network of complex topology with the Lightning-Induced Overvoltage (LIOV) toolbox of EMTP [27].

Starting from the promising results presented in [22], in this contribution the authors propose a novel set of three ML algorithms to regress lightning location and peak current from measurements of lightning-induced voltages. In particular, Deep Learning (DL) techniques are used.

The three algorithms, respectively labeled as “full frequency”, “full time domain” and “modified time domain” are first tested on the power system described in [22] (from now on labeled as “old scenario”); all of them reveal to be more effective than the one proposed in [22]. Then, the most performing algorithm among the three is then tested on a more realistic power system, i.e., a non linear three-phase distribution

line with the presence of Surge Arresters (SA), that will be indicated as “new scenario”.

A typical MV distribution line is selected for this purpose as the most probable application of the proposed tool (once fully developed) could be on such a type of system. This is due to a compromise between two necessities: (i) high spatial density for covering large regions with good location accuracy and (ii) the possibility of equipping the line with voltage sensors measuring in the order of tens or hundreds of kilovolts. Indeed, in Italy the density of distribution lines is significant (136 km/km², as reported by the Italian transmission system operator [28]) and they are typically equipped with SAs to mitigate the effect produced by intense lightning-induced over-voltages.

It is worth to mention that other ML applications exist in the field of lightning detection. For example, although conventional LLS classification is performed with multiparameter methods based on waveform characteristics, e.g., the Peak-To-Zero (PTZ) duration criterion [14], the use of ML for lightning classification purposes has been investigated in recent studies [29,30]. In particular, the authors of [30] developed a Supporting Vector Machine (SVM) model designed specifically for classifying Intra-Cloud (IC) and CG lightning pulses. Their algorithm achieves a 97% accuracy rate for IC(CG) classification (which is higher than that for the existing LLSs, i.e., 91%–96% [31]); moreover, it eliminates the need for manual waveform parameter extraction and estimates the accuracy of each prediction.

The layout of the paper is the following. Section 2 presents the three DL-based models capable of estimating both the location and the peak current of CG lightning strikes. The outcomes of our analysis on the “old scenario” are presented in Section 3. Section 4 outlines the details of the new scenario: power system, ground, lightning channel and current, and it presents the dataset of the lightning induced voltages simulated with the dedicated code LIGHT-PESTO [24]. The outcomes of our analysis on the “new scenario” are presented in Section 5. Lastly, we provide conclusions in Section 6.

2. Deep learning models

As previously stated, the three DL models are tested on the old scenario, while the best performing one's performances are assessed on the new one too.

All the proposed DL models require a preprocessing of the time domain signals and a dimensionality reduction, that are here described in detail. In all cases both the peak current and the stroke location are determined. From this point forward, the two voltage sensors recording the overvoltages are called VS1 and VS2 respectively, and the lightning-induced voltage waveforms observed at VS1 and VS2 are labeled v_1 and v_2 , respectively.

It is worth mentioning that the time scale of the approach does not contain leaders, continuing current, or other phases of the lightning flash development. We focus on the first return stroke phase only.

2.1. Full frequency domain method (FFDM)

Preprocessing raw data before giving them as input to DL algorithm is fundamental: in this specific case the time domain series must be transformed into a number of features, possibly reduced with respect to the time samples characterizing the voltage waveforms. In this case the waveform tails are basically a redundant information, since it is evident that most of the information is included in the first part of the transients. In [22], the authors removed from each couple of voltage waveforms the initial leading-zero values corresponding to the delay time between the initiation of the return stroke (simulated at $t = 0$) and the time of arrival of the induced-voltage at the closest voltage sensor, because in practical application one could just detect a voltage exceeding a specified threshold, while the return stroke initiation time would not be available. For this reason, also in this work, samples within the time interval corresponding to the pre-triggering of the

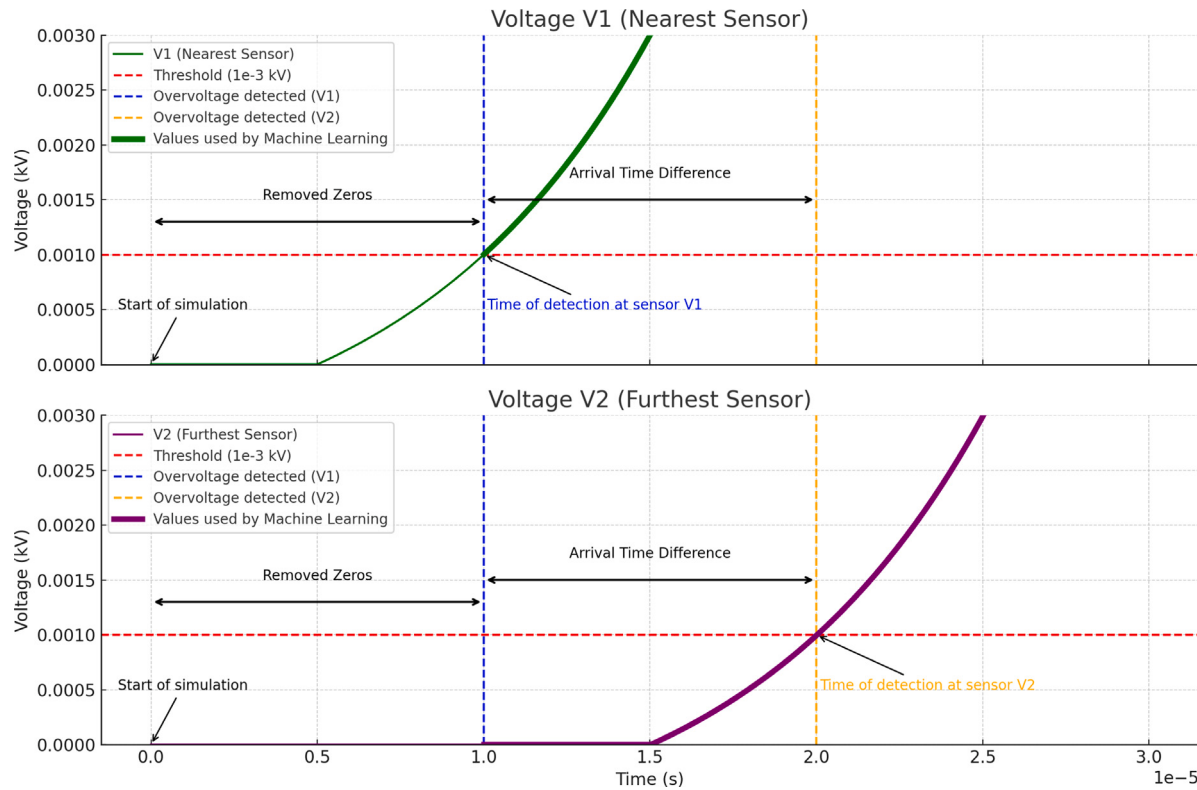


Fig. 1. Visualization of the preprocessing procedure with leading zero removal.

sensor closest to the lightning channel are removed from both v_1 and v_2 . This action creates vectors of different dimension; consequently, all the waveforms are truncated by removing points from the tail part, up to the size of the shortest waveform. As a result, the waveforms from VS1 are truncated to $n_1 < n$ time samples, and those from VS2 are truncated to $n_2 < n$ time samples, i.e. n_1 and n_2 may differ.

In order to further clarify the procedure described above, we can refer to Fig. 1: we remove the initial zero-valued samples from both waveforms up to the time when the nearest sensor first detects the event (i.e., when v_1 exceeds the threshold). We do not remove the values preceding the detection at the further sensor (v_2). This preprocessing step inherently retains the time difference between the arrival of the signals at the two sensors.

The Full Frequency Domain Method (FFDM) is characterized by a frequency based approach: the rationale behind this choice stems from the fact that fast transients are characterized by a higher frequency content than the mains frequency, especially during the first part of the waveform. This approach was followed also in [22], but in that work a Principal Component Analysis (PCA) was performed with the aim of further reducing the number of features. In this full frequency method, the whole frequency spectrum is considered. More in detail, the Discrete Fourier Transform (DFT) is applied to each voltage yielding a set of complex valued vectors; only values up to the Nyquist frequency are of course meaningful, the remaining ones are discarded. Finally, from each couple of vectors v_1 and v_2 , a single vector $\mathbf{X} \in \mathbb{R}^{n_F}$ (with $n_F = n_1 + n_2$) is obtained by stacking their real parts $\Re\{\text{DFT}(v_i)\}$ and their imaginary parts $\Im\{\text{DFT}(v_i)\}$. It is worth mentioning that translation (corresponding to the leading zeros removal) produces changes in the phase when working in the frequency domain; the FFDM uses both real and imaginary part of the samples, so the preprocessing procedure is effective also when working with this method. The vector \mathbf{X} is the feature vector that will be used by the algorithm to perform the current and location prediction. In particular, three different Neural Networks (NNs) are employed, respectively for the regression of the current I , the x and the y coordinate of the impact point.

2.2. Full Time Domain Method (FTDM)

The second method, referred to as Full Time Domain Method (FTDM) is, under the conceptual point of view, the simplest among the three, because the input features are simply time-time domain samples of the waveforms. The only preprocessing performed on the signals is the one previously described, i.e. the number of leading zeros at the beginning waveform closest to $t = 0$ are removed from both v_1 and v_2 , leading to feature vectors of dimensions n_1 and n_2 . The vectors v_1 and v_2 are stuck in a single vector \mathbf{X} , i.e., the feature vector that will be used as input to the three NNs for the regression of the three quantities I, x, y .

The use of time-domain rather than frequency-domain features to train the DL model leads to a set of features that, in principle, highlight the non periodic characteristic of the transient due to the nearby lightning strokes.

2.3. Modified Time Domain Method (MTDM)

The Modified Time Domain Method (MTDM) originates from the previous FTDM, with the main goal to achieve a dimensionality reduction, but at the same time retaining the characteristics of highlighting the non periodic behavior of the voltage signals. As in the other two methods, the first step of the preprocessing is performed by removing the leading zero samples, and the vectors acquired by VS1 (v_1) and VS2 (v_2) are unified to n_1 and n_2 samples.

To further reduce the number of features a compression operation is performed, leading to the new vectors \tilde{v}_1 and \tilde{v}_2 ; each of the time domain voltage vectors v_1 and v_2 is divided into two sections: the front section and the tail section. The initial section, clearly the more significant and informative, is compressed by a factor 3 described by Eq. (1) (applied to both vectors)

$$\tilde{v}_1(i) = \frac{1}{3} \sum_{k=0}^2 v_1(3i - k) \quad (1)$$

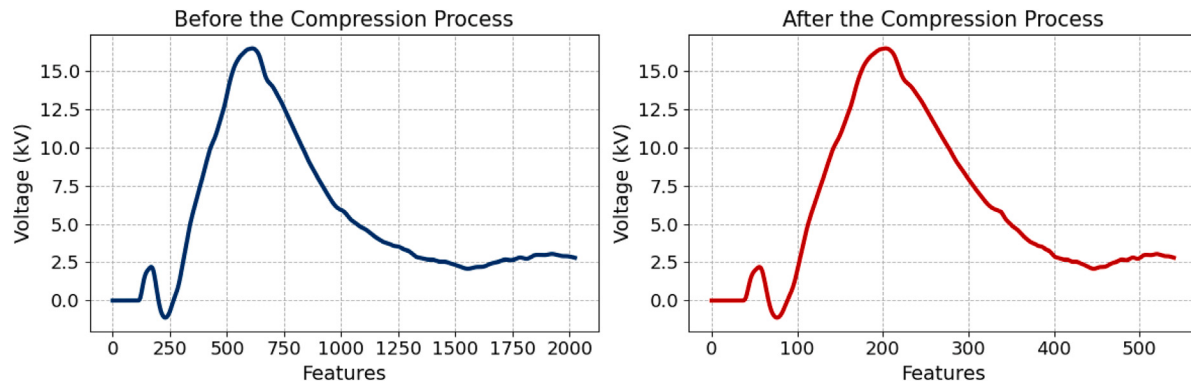


Fig. 2. Result of the compression operation. Voltage waveform observed at VS1, extracted from the dataset of the “New Scenario”. The peak current of the return stroke is 21 kA and the location is (1298 m, 660 m).

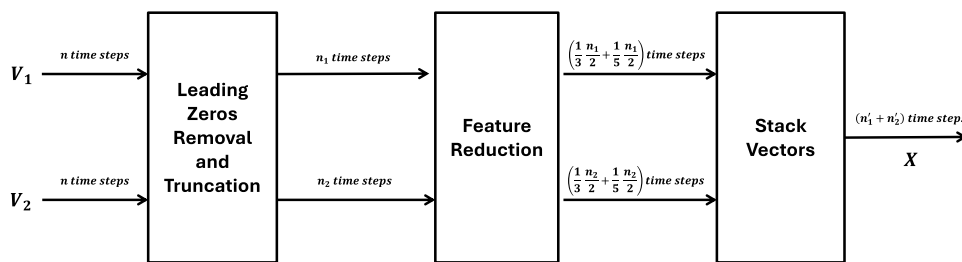


Fig. 3. Preprocessing and reduction procedure for modified time domain method.

i.e., every three neighboring time steps an averaging operation is performed. In the tail section, which is less critical, the averaging operation is performed every five time samples leading to a higher compression factor as shown in Eq. (2).

$$\tilde{v}_1(i) = \frac{1}{5} \sum_{k=0}^4 v_1(5i - k) \quad (2)$$

After a careful evaluation and different tests, the time domain signal is split into the initial and tail section in its mid point; consequently the number of elements in the voltage vectors v_1 and v_2 is reduced to $\frac{4n_1}{15}$ and $\frac{4n_2}{15}$, respectively.

Fig. 2 shows an example of two waveforms, before and after the compression process. It can be noticed that the waveforms maintain their main characteristics, but they are different in the number of samples (Features, x -axis). In addition, non homogeneous compression (lower in the first half of the waveform and higher in the second half) leads to a waveform distortion that can be seen by the different location of the peak value.

At the moment the distinction between the two sections is determined, as mentioned before, by identifying the mid point: this simple, yet effective, approach has the main rationale of being easy to implement and does not need any previous knowledge on the waveforms. Thinking about a practical implementation of the algorithm, this choice leads also to fast computation and training.

Finally, the feature vector X is created by stacking the modified \tilde{v}_1 and \tilde{v}_2 . The procedure for preprocessing and reducing feature numbers is illustrated in Fig. 3.

This feature vector will be used as input to the three NNs for the regression of the three quantities I, x, y . Such NNs share the same architecture but use distinct hyperparameters optimized for their specific task.

A sequential neural network model is implemented using Python’s Keras package. The model is trained with Stochastic Gradient Descent (SGD) and utilizes sigmoid activation functions in its hidden layers. To validate the model, 10-fold cross-validation is applied which is beneficial for enhancing model generalization and improving prediction

Table 1
Main characteristics of the three methods.

FFDM	FTDM	MTDM
Leading Zeros Removal	Leading Zeros Removal	Leading Zeros Removal
Fast Fourier Transform	Vectors Stacking	Compression Operation
Vectors Stacking	Neural Network	Vectors Stacking
Neural Network		Neural Network

performance. In 10-fold cross-validation, the entire dataset is divided into 10 equal parts (folds). Each time, 9 parts are used for training and 1 part for testing. This process is repeated 10 times so that each fold serves as the test set once. Thus, the cross-validation process ensures that 90% of the data is used for training and 10% for testing in each iteration. To optimize the hyperparameters, a randomized search technique is implemented, which involves sampling potential parameter values for the key hyperparameters such as learning rate, number of hidden layers, and number of neurons per hidden layer. The goal is to fine-tune the model by minimizing the Mean Squared Error, chosen as Loss Function. Table 1 shows a comparison “at a glance” of the three different methods.

3. Old scenario results: Comparison among the three methods

Since new DL algorithms are proposed in this work, their performances are evaluated firstly for a less complex scenario, which is that labeled as “Case 2” in [22]. The characteristics of the old scenario are summarized in Table 2.

The dataset is made of lightning-induced voltage waveforms observed where two voltage sensors are assumed to be installed and computed with the Lightning Power Electromagnetic Simulator for Transient Overvoltages (LIGHT-PESTO) [24]. With such a tool, realistic power systems with accurate models of power and protection devices, different values of ground conductivity, any current source at the base of the channel, and the well-known engineering models for the current attenuation along the channel [34] can be taken into account.

Table 2

Characteristics of the old scenario (that labeled as Case 2 in [22]) and the new scenario (presented in this work, Section 4).

	Old scenario	New scenario
Detection domain surface	100 km ²	10 km ²
Line length	10 km	2 km
Number of conductors	1	3
Number of sensors	2	2
Sensors position on the line	4 km, 6 km	0.5 km, 1.5 km
Line terminations	498 Ω	498 Ω
SA (span)	No (n.a.)	Yes (250 m)
Channel base current	Heidler's first return stroke [32]	Heidler's first return stroke [32]
Channel height	8 km	8 km
Return stroke speed	0.4 c ₀	0.4 c ₀
Current attenuation model	MTLE [33]	MTLE [33]
Soil conductivity	5 mS/m	1 mS/m
Time window	66.7 μs	37.0 μs
Time discretization step	100 ns	10 ns
Line discretization step	90 m	9 m
Number of samples	2000	2000
Size of voltage waveform vectors	668	3701
Induced voltage simulation	LIGHT-PESTO [24]	LIGHT-PESTO [24]
Random lightning location	Uniform distribution	Uniform distribution
Random peak current	Lognormal distribution [6]	Lognormal distribution [6]

In this scenario, lightning events are simulated assuming a random peak current with a log-normal distribution and considering the lossy ground case. It is worth to highlight that the quantity which is used for the training of the models is the lightning-induced voltage, and not the electromagnetic fields as done by conventional LLS. Thus, in operations, data will be collected by voltage sensors installed on overhead distribution lines and activating with overvoltages higher than a threshold value (e.g., 10 V in accordance with [26]).

The optimal neural network architecture for the MTDM comprises three hidden layers, with each layer containing 74 neurons, while regarding the other two methods (FTDM and FFDM), the best results were obtained with two hidden layers with 128 and 64 neurons respectively. The layers are fully connected, with sigmoidal activation functions for MTDM and ReLU activation functions for FTDM and FFDM.

In the following evaluations, the Mean Absolute Error (MAE) is calculated; its definition is reported in (3) for the current, in which \hat{I} is the predicted current while I is the ground truth

$$MAE = \frac{1}{N} \sum_{k=1}^N |\hat{I}_k - I_k| \quad (3)$$

As depicted in Fig. 4, the R^2 values for the predicted current and coordinates across all three approaches are remarkable, approaching unity. It indicates a robust alignment of the models with the data. To better appreciate the relative error, in the case of the current the Mean Absolute Relative Error (MAPE) was also calculated as:

$$MAPE = \frac{1}{N} \sum_{k=1}^N \left| \frac{\hat{I}_k - I_k}{I_k} \right|. \quad (4)$$

The current errors are remarkably low, with values of 0.81 kA MAE (2.38% MAPE) for the MTDM, 0.89 kA MAE (3.03% MAPE) for the FTDM, and 1.00 kA MAE (3.65% MAPE) for the FFDM. Although there are slight variations, the error amounts across all three approaches are relatively similar. The notable difference among these three approaches becomes evident in the prediction results for coordinates x and y . While the accuracy of the FFDM and FTDM approaches is approximately the same (the MAE is around 110 m for the x coordinate prediction), the MTDM stands out with a notably decreased MAE by half, at 57 m. Similarly, for the prediction of the y coordinate, the accuracy of the MTDM ($MAE = 98.96$ m) surpasses that of the FFDM ($MAE = 114.55$ m), and the FFDM outperforms the full-time domain approach ($MAE = 137.65$ m).

In Fig. 5, the scatter plot illustrates lightning spots within the observation domain, where each spot's size and color correspond to

Table 3
Performance comparison for the old scenario.

	FFDM	FTDM	MTDM
MAE _I (kA)	1.00	0.89	0.81
MAE _x (m)	114.17	1106.38	57.09
MAE _y (m)	114.55	137.65	98.96
ALE (m)	179.73	192.91	133.58

its location error $\|\hat{\mathbf{p}}_k - \mathbf{p}_k\|$, where $\|\cdot\|$ stands for the Euclidean distance between the predicted location $\hat{\mathbf{p}}$ and the real location \mathbf{p} . This visualization is provided for all three approaches. Notably, in the MTDM, the circles are visibly smaller, indicating a lower location error compared to the other approaches. Additionally, the number of outliers near the line $y = 0$ appears to be higher in the FTDM and FFDM compared to the MTDM.

Fig. 6 shows the Average Location Error (ALE), calculated as

$$ALE = \frac{1}{N} \sum_{k=1}^N \|\hat{\mathbf{p}}_k - \mathbf{p}_k\|. \quad (5)$$

The histogram of location errors, also shown in Fig. 6 demonstrates that the MTDM leads to a reduction of the location error by approximately 30% if compared to the FTDM, decreasing from 192.91 m to 133.58 m. Additionally, the histogram relative to the FTDM reveals a tighter clustering of points towards lower location errors, indicating a higher concentration of data points in this region. Around 57% of samples exhibit location errors of lower than 100 m in this approach. Conversely, in the two other approaches, the distribution appears to spread out more evenly across the range, with a flatter peak situated closer to higher location errors, and only about 37% percent demonstrate less than 100 m location error.

A summary of the results of this comparison is reported in Table 3.

4. The new scenario: Characteristics and voltage database creation

The data for the creation of the new scenario database are obtained via simulation using a dedicated code (i.e., LIGHT-PESTO [24]), whose characteristics are briefly summarized in the following. LIGHT-PESTO, which is developed in the Matlab-Simulink environment, aims at solving two problems, in the presented order: (i) the computation of return

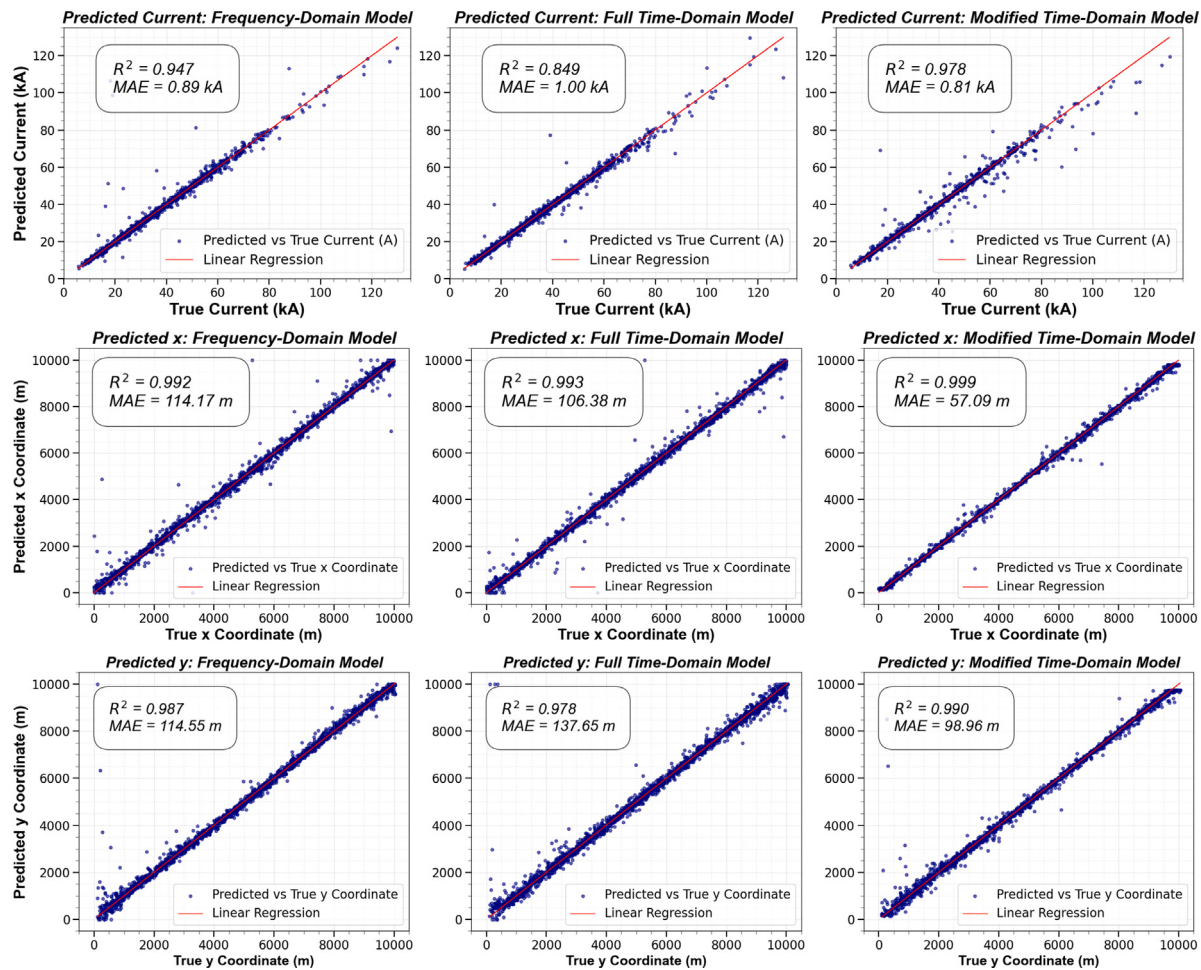


Fig. 4. Scatter plots of predicted parameters for the old scenario using the three prediction approaches.

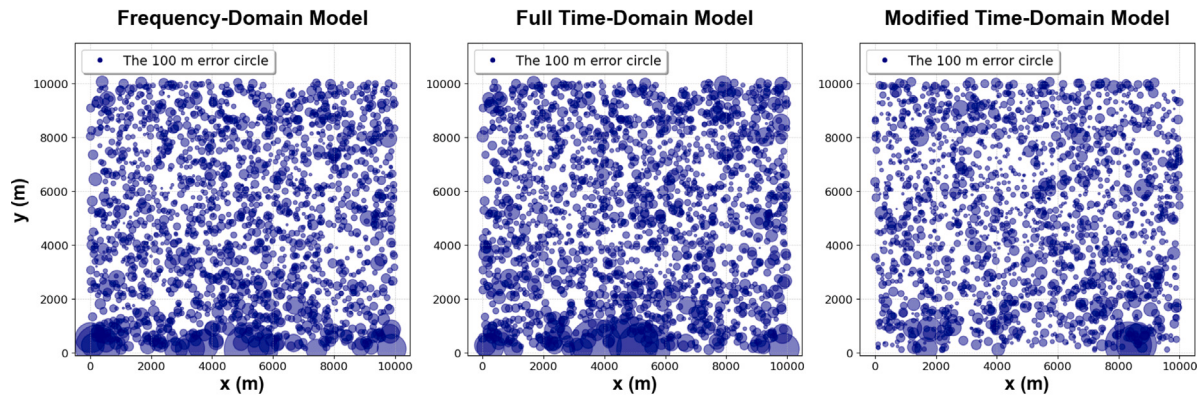


Fig. 5. Scatter diagrams of simulated lightning events within the detection area using three approaches for the old scenario. The size and color of each marker represent the location error, providing insights into the accuracy of event localization. The detection domain is $10 \times 10 \text{ km}^2$, the 10-km long transmission line is located along the x -axis [22].

stroke EM fields in the free space; (ii) the solution of the field-to-line coupling problem.

As far as the EM fields evaluation, the semi-analytical approach proposed in [35] is implemented in the code. Such method does not involve any assumption either on the channel-base current waveshape or on the attenuation function of the current along the channel. Integrands are developed in series of exponential functions (Prony series) which makes them analytically solvable. To consider the lossy ground case, the Cooray-Rubinstein correction [36,37] of the radial component of the electric field is implemented according to the approach

presented in [38], i.e., superimposing the contribution provided by different segments of the channel calculated, again, through the Prony expansion. With respect to the method simply performing numerical integrations (Gaussian quadrature) starting from the time-domain formulas proposed in [39], such an approach allows to reduce the CPU time of a factor from 20 (lossy ground) to some hundreds (PEC ground), for typical return stroke models.

The solution of the field-to-line coupling problem is based on the second-order FDTD scheme of the Agrawal model [40]. The input is the EM fields and the output is the update of the voltages and of

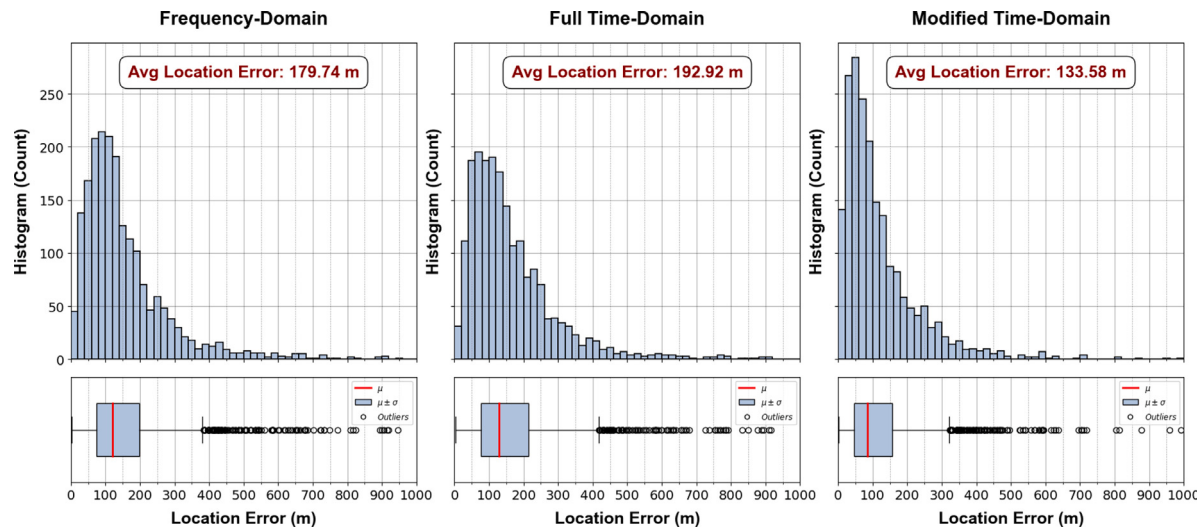


Fig. 6. Histogram of location error distribution for the old scenario.

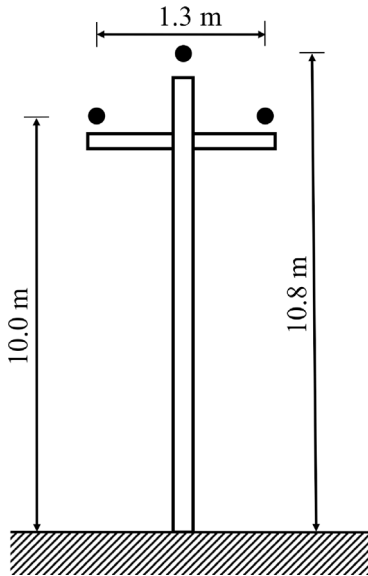


Fig. 7. Three-phase distribution system geometry.

the currents in all the internal points of the line, according to the discretization. The code implementation is adapted from the approach proposed in [4] which is interfaced with the PSCAD-EMTDC platform and is able to consider realistic power networks with complex topology and automatically distinguish between direct and indirect lightning strikes.

The characteristics of the new scenario are summarized in Table 2. In what follows, all details regarding the generation of a database of lightning-induced voltages on such a power system are provided.

4.1. Distribution line

The length of the line and its complexity, as well as the extension of the simulation domain are determined with a compromise between the system performance in coordinates location and peak current regression, and the computational cost associated with generating the voltage dataset. A 2-km long straight distribution line (without laterals) made of three conductors (three-phase system without neutral) equipped with Surge Arresters (SA) is considered. The geometry of the line is

depicted in Fig. 7 (the same configuration of [41]). The diameter of the conductors is assumed to be 2 cm. The terminations at the line ends are chosen to minimize reflections (matched case, the termination resistances equals the line characteristic impedance, i.e., 498Ω). SA are placed at the line discontinuities. According to the results shown in [41], effective line protection is achieved by placing the SA at intervals of less than 300 m. Thus, in this study, we consider a 2-km distribution line with SA installed every 250 m on each phase at insulators.

4.2. Simulation domain

The simulation domain covers an area of 10 km^2 , as shown in the schematic representation reported in Fig. 8. It extends along the MV line for 1 km (in the central portion $500 \text{ m} \leq x \leq 1500 \text{ m}$, to avoid edge effects) and transversely to the line for 5 km in both directions. Two Voltage Sensors (VS1 and VS2) are placed at the pylons at $x = 500 \text{ m}$ and $x = 1500 \text{ m}$, respectively. It is worth to note that, since the system is symmetric, the same signal corresponds to two lightning strike points, that are (x, y) and $(x, -y)$. The ambiguity could be removed in practical applications by using a signal from a sensor on another line or considering the presence of some elements in the detection region making the systems asymmetric.

4.3. Surge arresters

SA are protective devices that limit line voltage by connecting each phase to the ground when a surge current flows through the conductors. The V-I characteristic of SA in non-linear; thus, to include the effects produced by the presence of such devices in the LIGHTPESTO code [24] we use the equivalent circuit reported in Fig. 9 which is adapted from the model proposed in [43]. The circuit model is characterized by three resistances (R , R_{A0} and R_{A1}), two inductances (L_0 and L_1), and two nonlinear resistances (A_0 and A_1). These parameters are defined as follows. The resistance R is set equal to $1 \text{ M}\Omega$ and used to overcome numerical errors [43]. R_{A0} (R_{A1}) is connected in parallel to the non-linear resistor A_0 (A_1) and is set equal to $1 \text{ G}\Omega$ to avoid voltage pulses across the inductors. The inductances are calculated starting from the data sheet of the SA based on the expressions made available in [43]. Assuming a 20-kV MV line, we consider the SBKC 24/SL-0 model produced by Tridelta Meidensha, whose nominal voltage is 24 kV [44]. From residual voltage data associated with various test impulse currents, it is possible to set $L_0 = 0.5172 \text{ mH}$ and $L_1 = 0.1724 \text{ mH}$.

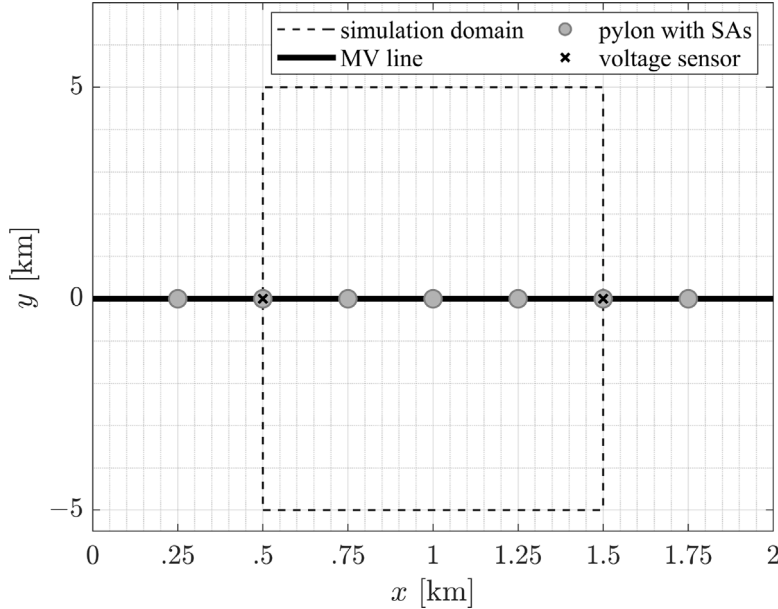


Fig. 8. Scheme of the MV line and of the lightning simulation domain.

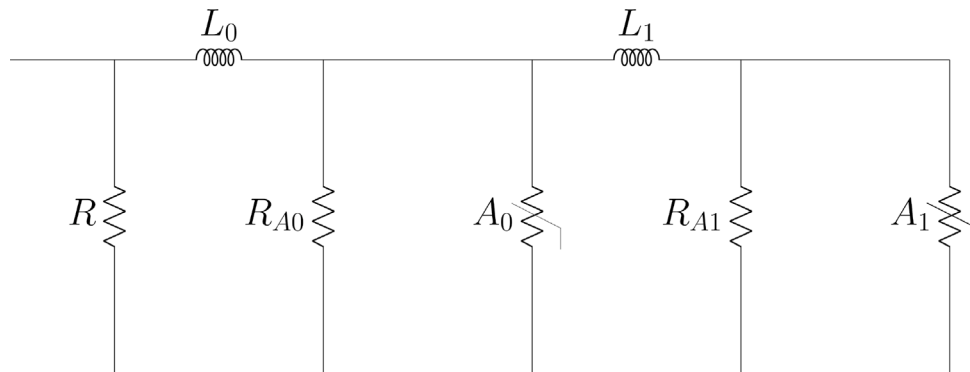


Fig. 9. Surge arrester equivalent circuit.

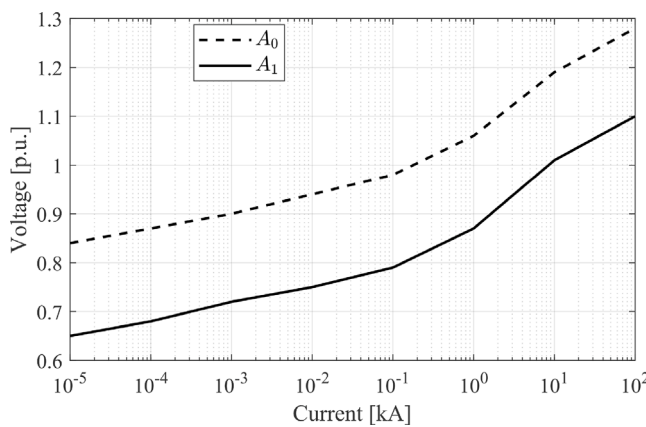


Fig. 10. Surge arrester, V-I characteristic of non-linear resistances proposed in [42].

The two non-linear resistances are defined by the V-I characteristic proposed in [42] and shown in Fig. 10. The voltage is expressed in per unit on the base $V_{r8/20} = 63.8$ kV, as available in the data sheet of the commercial SA. Such a value is the residual voltage associated with a peak impulse current of 10 kA with rising front time of 8 μ s

and time at half-value of 20 μ s. In analogy with the model proposed in [43], the insulator to which a SA is placed in parallel is modeled as a capacitor with a capacity equal to 1 pF, connected to the ground thorough a resistance of 120 Ω , as the one adopted in [45].

4.4. Lightning discharge model

This subsection presents the lightning discharge model considered in this work, which is that used also in [22]. The lightning channel is assumed as a straight vertical thin-wire radiator with a height $H = 8$ km. The current source, that is injected at the base of the channel, is modeled with the Heidler's function [32] in which the parameters are set to reproduce a typical negative first return stroke channel-base current. The return stroke current propagates upward along the channel with a speed equals to 40% the speed of light in vacuum ($c_0 = 3 \cdot 10^8$ m/s) and attenuates according to the Modified Transmission Line model with Exponential decay (MTLE) [33].

4.5. Soil

LIGHT-PESTO allows to consider a uniform soil with any conductivity value. For the test cases here proposed, we consider the lossy ground case assuming a 1-mS/m conductivity and a relative permittivity equal to 10.

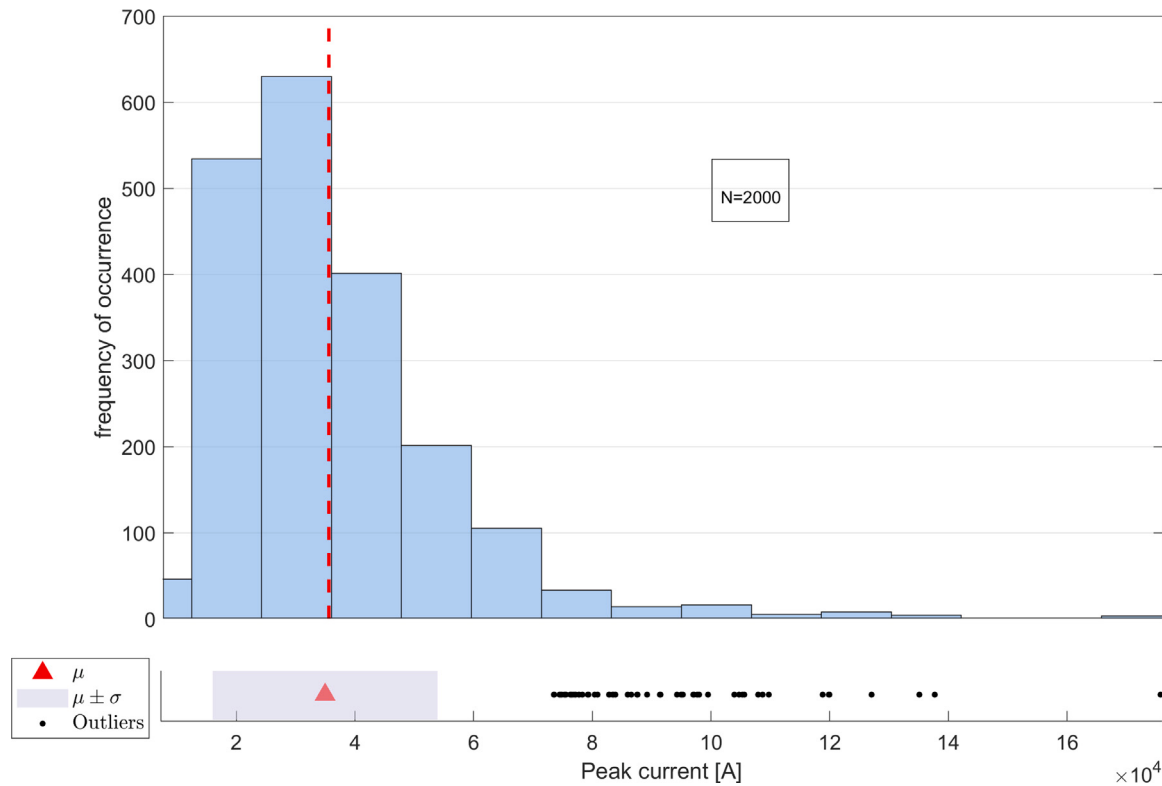


Fig. 11. Peak current distribution of the $N = 2000$ generated lightning events.

4.6. Simulation setup

An accurate computation of the transients produced by the presence of SA requires the selection of a fine time step dt ; thus in this work we set it equal to 10 ns. The considered time window is $[0, T]$, where $T = 37 \mu\text{s}$ is the time needed by the electromagnetic fields generated by a lightning strike at one of the corners of the simulation domain to reach the most distant sensor, i.e. $\frac{\sqrt{3^2+1^2}\cdot 10^3}{c_0} \approx 17 \mu\text{s}$, plus the time necessary for the observation of the evolution of the lightning-induced voltage on the line, that is assumed equal to 20 μs . It is worth to note that this value is lower than the limit of validity of the current propagation model, i.e., $T_{\max} = H/(0.4 c_0) = 66.7 \mu\text{s}$. The line discretization step $dx = 3 c_0 dt = 9 \text{ m}$ is selected by combining the Courant's stability condition with the method of characteristics [46].

4.7. Lightning-induced voltage dataset

$N = 2000$ random lightning strikes are simulated within the simulation region. For each event the coordinates of the point of impact are extracted using a uniform distribution, whereas the current peak is extracted according to the log-normal distribution which is typically applied in the literature for negative first return strokes (i.e., median value: 31.1 kA; logarithmic standard deviation: 0.484 kA [6]). The peak current distribution of the generated lightning events is shown in Fig. 11.

In the simulation code, a filter codifying the well-known Electro-Geometric Model (EGM) [47] is implemented to discriminate if the lightning event results in a direct or an indirect strike (i.e., due to coupling process between lightning EM fields and the line). Of course, direct strikes are close to the line and/or characterized by high values of peak current. Such samples are discarded and replaced. This because the direct strike process is completely different, so a dedicated model should be implemented. Moreover, direct events are much less frequent; thus, we believe that for the purposes of the work, only the induced effect can be taken into account.

The output of each simulation consists of two voltage waveforms observed by the two voltage sensors. Fig. 12 show some examples of voltage waveforms making the dataset. The size of the voltage waveform vectors is $n = 1 + T/dt = 3701$, thus more than 5 times higher than that used in the training set of the model proposed in [22]. As will be detailed in the next section, this leads to a curse of dimensionality, which, together with the non-linear effects generated by the presence of SA, requires the adoption of a more sophisticated approach for the development of a novel algorithm able to regress the lightning location and the peak current with good accuracy.

5. New scenario results

As demonstrated in the previous section, the prediction results obtained from the MTDM outweighs those of the other two methodologies. Consequently, this approach has been selected for implementation with the new scenario.

5.1. MTDM for the new scenario

As mentioned earlier, this new dataset includes 2000 simulated random lightning strikes within the simulation region, assuming a random peak current with a log-normal distribution.

The optimal neural network architecture consists of three hidden layers with 74 neurons each. Following the same approach used for the old scenario, where the entire dataset ($N = 2000$) is used as the test set, 10-fold cross-validation is implemented.

Although the number of features is significantly higher in this new scenario, and the curse of dimensionality is expected, Fig. 13 demonstrate that both the R^2 and MAE values for predicted current and coordinates confirm the excellent fit to the data. The MAE values are notably low at 14.01 m for the x -coordinate and 59.58 m for the y -coordinate, reflecting the robustness of the approach even with a high number of input features.

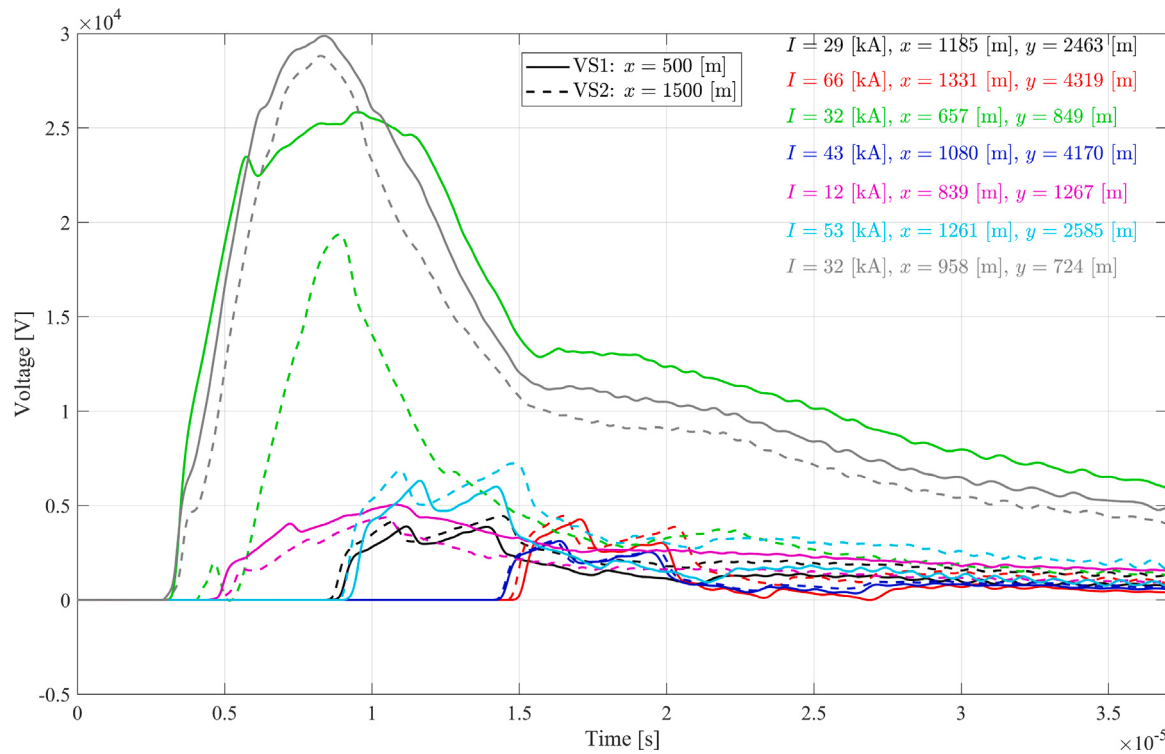


Fig. 12. Dataset extract; voltages measured by VS1 ($x = 500$ m) in solid line, voltages measured by VS2 ($x = 1500$ m) in dashed line. The peak current I and the coordinates (x, y) of the strike location are specified for each event reported.

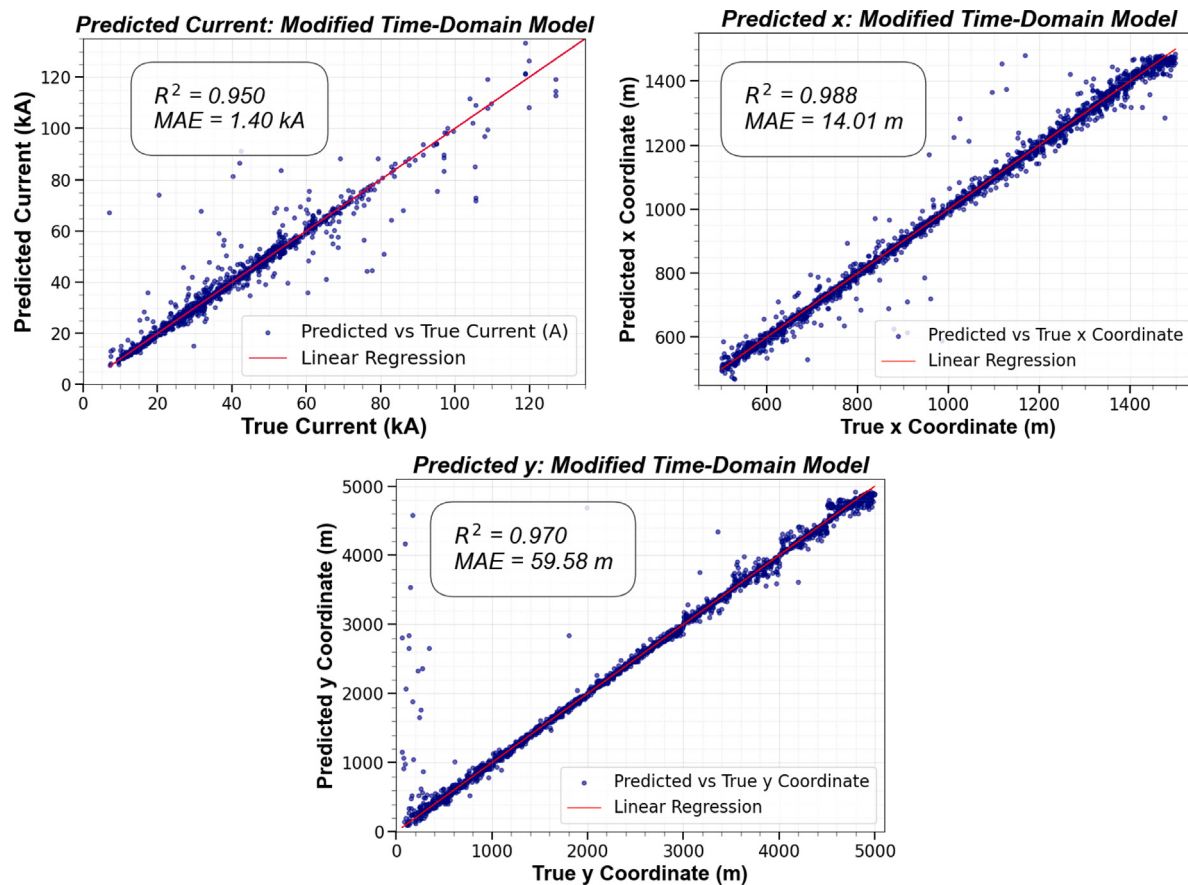


Fig. 13. Scatter plots of predicted parameters for the new scenario using MTDM.

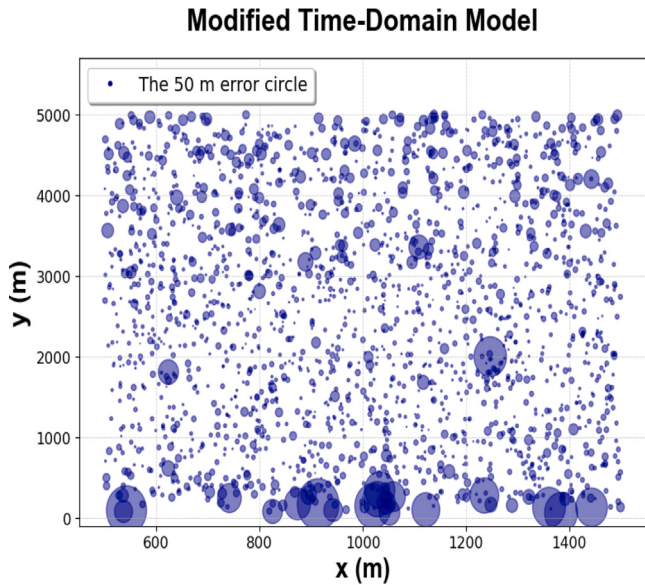


Fig. 14. Scatter diagram of simulated lightning events within the new scenario detection domain illustrated in Fig. 8. The 2-km long distribution line is located along the x -axis. The size and color of each marker represent the location error, providing insights into the accuracy of event localization.

The scatter plot of lightning spots (Fig. 14) of location errors reveals that the location errors for most spots are below 50 m. The histogram of location errors (Fig. 15) reports an average value of 67.24 m and indicates that approximately 70% of samples have errors lower than 50 m.

These results are promising; however, consistently with the last panel of Fig. 13, it can be observed that a small number of large location errors are distributed near to the line where the voltage sensors are placed, hence with low y -values. Such outliers are due to physics of the system. Indeed, the exact analytical dependence of the lightning-induced voltage on the distance between the point of impact and the line is difficult to calculate since it needs to compute lightning electromagnetic fields and then to solve the Maxwell's equations describing the field-to-line coupling problem. However, simplified methods provided the induced voltage peak with an approximated formula that is linear [23] or quadratic [48] with respect to the inverse of such a distance. Thus, near the line, small y -variations can result in considerable variations in the induced voltage, and this may affect the capability of the model to regress the y -coordinate. Although with less impact, the same behavior can be observed also in the old scenario results.

5.2. Robustness analysis of MTDM in presence of noise

In the realistic experimental data, noise is present, whereas the simulated voltage waveform is noise-free. To assess the effect of noise on the prediction results, Additive White Gaussian Noise (AWGN) is added to the simulated time-domain voltage waveform, and then the model is trained using these noisy data. Table 4 presents results with two different levels of noise. Despite these noise levels being much higher than typical realistic measurement noise, the impact on the predicted data is not significant. Comparing this result with the ones reported in [22], it is evident that the detrimental effect caused by the presence of noise is reduced. This suggests that using a time-domain approach characterized by an averaging process, instead of a frequency-domain approach has reduced the model's sensitivity to noise.

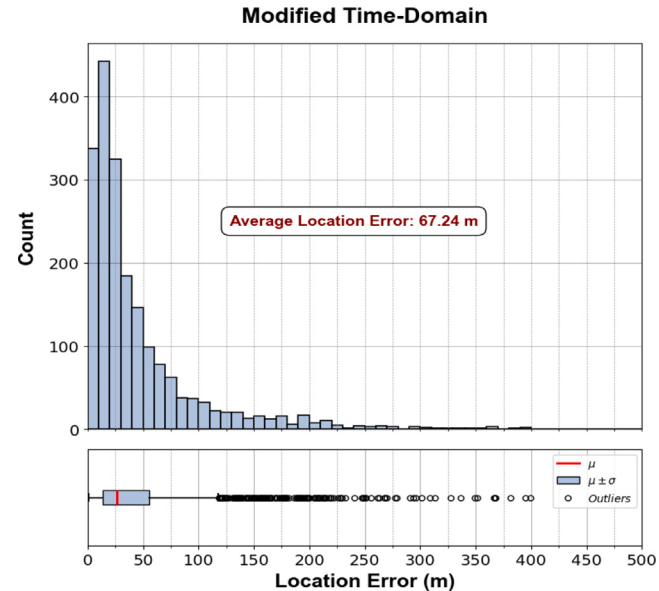


Fig. 15. Histogram of location error distribution for the new scenario.

Table 4

Assessing the impact of incorporating noise into the simulation dataset on the prediction outcomes with MTDM on the new scenario.

	Noise 1	Noise 2
SNR (dB)	25.14	39.11
Max noise (V)	500	100
MAE_I (kA)	2.31	2.00
MAE_x (m)	30.02	18.57
MAE_y (m)	93.44	74.22
ALE (m)	105.18	82.84

Table 5

Comparison between MTDM performance trained considering two different soil conductivity values and the same power system ("New Scenario").

	$\sigma = 1$ mS/m	$\sigma = 5$ mS/m
MAE_I (kA)	1.40	1.22
MAE_x (m)	14.01	22.22
MAE_y (m)	59.58	59.99
ALE (m)	67.24	72.73

5.3. Effects of the soil conductivity on MTDM

The soil conductivity mostly affects the radial component of the lightning electric field, which is the source term of the field-to-line coupling differential equations. In [22], a comparison was proposed between the results of the same ML model trained considering lightning-induced voltages with two different soil conductivity values, and no major variations were detected (location error 290 m and 270 m with $\sigma = 10$ mS/m and $\sigma = 5$ mS/m, respectively). In this framework, we perform the same experiment using MTDM on the new scenario. Observing the results reported in Table 5, it can be concluded that changing the soil conductivity does not significantly affect the accuracy of the model (it is worth stressing that the same NN is re-trained considering lightning-induced voltages with a different soil conductivity value, i.e., $\sigma = 5$ mS/m instead of $\sigma = 1$ mS/m).

Finally, a discussion on the effects of the grounding conditions on the regression model is necessary. The number of events inside the considered detection domain (10 km^2) causing the activation of SAs (and so a discharge current flowing across the grounding system) are few and thus likely not to impact on the training of the ML model. Moreover, whereas the soil characteristics in the region around the line are typically estimated with some approximations, for a given line, the

grounding system which is installed is known, so the algorithm can be easily optimized for that particular grounding condition.

6. Conclusion

The paper presented three new Machine Learning (Deep Learning) models able to regress both the position and the channel base current peak of a lightning event, starting from the measurement of the overvoltages induced on a (multiconductor) transmission or distribution line system, even with the presence of non-linear devices (surge arresters). The first algorithm works in the frequency domain but, contrarily to a previously developed model, it makes use of the whole frequency spectrum. The other two methods directly take the time domain sequence and differentiate each other because of different recipes to produce the final features vector. All the methods reveal to be outperforming with respect to the previously developed one; the most effective one was also tested on a more realistic power system, highlighting performances which can be competitive with conventional lightning location systems, i.e., average location error from 67.24 m to 105.18 m and mean absolute error on the peak current from 1.22 kA to 2.31 kA, considering different soil conductivity values and different noise level on data (SNR down to 25.14 dB). Future work will concern the possibility of performing experimental validation of the developed methods starting first with reduced scale system to end up with real transmission or distribution networks equipped with voltage sensors. Moreover, we will extend the approach to different lightning types and face the problem of identifying if a particular voltage signal recorded by a sensors is due to an indirect or direct strike and classifying the source. This may also provide useful information to be integrated within LLS identification and classification algorithms.

CRediT authorship contribution statement

Shayan Dodge: Writing – original draft, Software, Methodology, Investigation, Data curation. **Martino Nicora:** Writing – original draft, Visualization, Software, Methodology, Data curation. **Sami Barmada:** Writing – review & editing, Supervision, Project administration, Methodology, Conceptualization. **Massimo Brignone:** Writing – review & editing, Supervision, Software, Formal analysis, Conceptualization. **Renato Procopio:** Writing – review & editing, Supervision, Project administration, Methodology, Conceptualization. **Mauro Tucci:** Writing – review & editing, Validation, Software, Methodology, Formal analysis.

Declaration of competing interest

The authors declare the following financial interests/personal relationships which may be considered as potential competing interests: Renato Procopio reports financial support was provided by Italian Ministry for Education, University, and Research. Nicora, Brignone, Procopio, Barmada, Tucci has patent Metodo e sistema per la rilevazione di eventi di fulminazione in un'area di interesse pending to University of Genoa and University of Pisa. If there are other authors, they declare that they have no known competing financial interests or personal relationships that could have appeared to influence the work reported in this paper.

Acknowledgments

This work was partially supported by the Italian Ministry for Education, University, and Research under the project PRIN 2022, grant number 20224CL7HM, and the European Union- Next Generation EU.

Data availability

Data will be made available on request.

References

- [1] V. Rakov, M. Uman, *Lightning: Physics and Effects*, Cambridge University Press, 2003.
- [2] M. Nicora, D. Mestriner, M. Brignone, R. Procopio, E. Fiori, A. Piantini, F. Rachidi, Estimation of the lightning performance of overhead lines accounting for different types of strokes and multiple strike points, *IEEE Trans. Electromagn. Compat.* 63 (6) (2021) 2015–2023, <http://dx.doi.org/10.1109/TEMC.2021.3060139>.
- [3] M. Nicora, D. Mestriner, M. Brignone, M. Bernardi, R. Procopio, E. Fiori, F. Delfino, A. Piantini, F. Rachidi, Assessment of the lightning performance of overhead distribution lines based on lightning location systems data, *Int. J. Electr. Power Energy Syst.* 142 (2022) 108230, <http://dx.doi.org/10.1016/j.ijepes.2022.108230>.
- [4] M. Brignone, F. Delfino, R. Procopio, M. Rossi, F. Rachidi, Evaluation of power system lightning performance - Part II: application to an overhead distribution network, *IEEE Trans. Electromagn. Compat.* 59 (1) (2017) 146–153, <http://dx.doi.org/10.1109/TEMC.2016.2601657>.
- [5] A. Borghetti, C.A. Nucci, M. Paolone, Indirect-lightning performance of overhead distribution networks with complex topology, *IEEE Trans. Power Deliv.* 24 (4) (2009) 2206–2213, <http://dx.doi.org/10.1109/TPWRD.2009.2021038>.
- [6] IEEE, Guide for improving the lightning performance of electric power overhead distribution lines, in: IEEE Std. 1410-2010 (Revision of IEEE Std 1410-2004), 2011, pp. 1–73, <http://dx.doi.org/10.1109/IEESTD.2011.5706451>.
- [7] S.K. Clark, D.S. Ward, N.M. Mahowald, Parameterization-based uncertainty in future lightning flash density, *Geophys. Res. Lett.* 44 (6) (2017) 2893–2901, <http://dx.doi.org/10.1002/2017GL073017>.
- [8] M. Lagasio, A. Parodi, R. Procopio, F. Rachidi, E. Fiori, Lightning Potential Index performances in multimicrophysical cloud-resolving simulations of a back-building mesoscale convective system: The Genoa 2014 event, *J. Geophys. Res.: Atmos.* 122 (8) (2017) 4238–4257, <http://dx.doi.org/10.1002/2016JD026115>.
- [9] A. La Fata, F. Amato, M. Bernardi, M. D'Andrea, R. Procopio, E. Fiori, Cloud-to-Ground lightning nowcasting using Machine Learning, in: 35th International Conference on Lightning Protection (ICLP) and XVI International Symposium on Lightning Protection, Vol. 1, SIPDA, 2021, pp. 1–6, <http://dx.doi.org/10.1109/ICLPandSIPDA54065.2021.9627428>.
- [10] A. La Fata, F. Amato, M. Bernardi, M. D'Andrea, R. Procopio, E. Fiori, Horizontal grid spacing comparison among Random Forest algorithms to nowcast Cloud-to-Ground lightning occurrence, *Stoch. Env. Res. Risk. Assess.* 36 (2022) 2195–2206, <http://dx.doi.org/10.1007/s00477-022-02222-1>.
- [11] G. Diendorfer, Lightning location systems (LLS), in: Proc. IX Int. Symp. on Light. Prot. (SIPDA), Foz do Iguaçu, Brazil, 2007.
- [12] W. Schulz, G. Diendorfer, S. Pedeboy, D.R. Poelman, The European lightning location system EUCLID - Part 1: performance analysis and validation, *Nat. Hazards Earth Syst. Sci.* 16 (2) (2016) 595–605, <http://dx.doi.org/10.5194/nhess-16-595-2016>.
- [13] V.P. Idone, A.B. Saljoughy, R.W. Henderson, P.K. Moore, R.B. Pyle, A reexamination of the peak current calibration of the national lightning detection network, *Geophys. Res. Atmos.* 98 (D10) (1993) 18,323–18,332, <http://dx.doi.org/10.1029/93JD01925>.
- [14] G. Diendorfer, M. Bernardi, K. Cummins, F. De La Rosa, B. Hermoso, A. Hussein, T. Kawamura, F. Rachidi, V. Rakov, W. Schulz, H. Torres, Cloud-to-Ground Lightning Parameters Derived from Lightning Location Systems – The Effects of System Performance (CIGRE TR C4.404), Electra, CIGRE, 2009.
- [15] K. Berger, R.B. Anderson, H. Kroninger, Parameters of lightning flashes, *Electra* 41 (1975) 23–37.
- [16] S. Visacro, A. Soares Jr., M.A.O. Schroeder, L.C.L. Cherchiglia, V.J. de Sousa, Statistical analysis of lightning current parameters: Measurements at Morro do Cachimbo Station, *J. Geophys. Res.: Atmos.* 109 (D1) (2004) 1–11, <http://dx.doi.org/10.1029/2003JD003662>.
- [17] G. Diendorfer, M. Mair, W. Schulz, W. Hadrian, Lightning current measurements in Austria - Experimental setup and first results, in: 25th ICLP (International Conference on Lightning Protection), 2000, pp. 44–47.
- [18] F. Fuchs, E. Landers, R. Schmid, J. Wiesinger, Lightning current and magnetic field parameters caused by lightning strikes to tall structures relating to interference of electronic systems, *IEEE Trans. Electromagn. Compat.* 40 (4) (1998) 444–451, <http://dx.doi.org/10.1109/15.736205>.
- [19] W. Janischewskyj, A. Hussein, V. Shostak, I. Rusan, J.-X. Li, J.-S. Chang, Statistics of lightning strikes to the Toronto Canadian National Tower (1978–1995), *IEEE Trans. Power Deliv.* 12 (3) (1997) 1210–1221, <http://dx.doi.org/10.1109/61.636949>.
- [20] A.J. Eriksson, Lightning and tall structures, *Trans. South Afr. Inst. Electr. Eng.* 69 (8) (1978) 238–252.

- [21] H. Karami, A. Mostajabi, M. Azadifar, M. Rubinstein, C. Zhuang, F. Rachidi, Machine learning-based lightning localization algorithm using lightning-induced voltages on transmission lines, *IEEE Trans. Electromagn. Compat.* 62 (6) (2020) 2512–2519, <http://dx.doi.org/10.1109/TEMC.2020.2978429>.
- [22] M. Nicora, M. Tucci, S. Member, S. Barmada, M. Brignone, R. Procopio, Lightning location and peak current estimation from lightning-induced voltages on transmission lines with a machine learning approach, *IEEE Trans. Electromagn. Compat.* (2024) <http://dx.doi.org/10.1109/TEMC.2024.3375452>.
- [23] S. Rusck, *Induced-Lightning Overvoltages on Power Transmission Lines with Special Reference to the Overvoltage Protection of Low Voltage Networks*, KTH, Stockholm, 1958.
- [24] L. Farina, D. Mestriner, R. Procopio, M. Brignone, F. Delfino, The lightning power electromagnetic simulator for transient overvoltages (LIGHT-PESTO) code: A user-friendly interface with the MATLAB-Simulink environment, *IEEE Lett. Electromagn. Compat. Pr. Appl.* 2 (4) (2020) 119–123, <http://dx.doi.org/10.1109/LEMCPA.2020.3032180>.
- [25] S. Barmada, M. Tucci, M. Brignone, M. Nicora, R. Procopio, Neural Network Based Procedure for Lightning Localization, in: Presented At the 37th International Conference on Lightning Protection (ICLP), Dresden, Germany [Proceedings Forthcoming], 2024.
- [26] M. Asadi, N. Ravichandran, S. Rajabi, T. Miki, H. Karami, M. Rubinstein, F. Rachidi, A. Andreotti, Single-Sensor Machine-Learning-Based Lightning Localization using Lightning-Induced Voltages, in: Presented At the 37th International Conference on Lightning Protection (ICLP), Dresden, Germany [Proceedings Forthcoming], 2024.
- [27] F. Napolitano, A. Borghetti, C.A. Nucci, M. Paolone, F. Rachidi, J. Mahseredjian, An advanced interface between the LIOV code and the EMTP, in: Proceedings of 29th International Conference on Lightning Protection, ICLP, Uppsala, Sweden, 2008.
- [28] Terna, *Valutazione Ambientale del Piano di Sviluppo della Rete Elettrica di Trasmissione Nazionale 2008, 2007*.
- [29] J. Wang, Q. Huang, Q. Ma, S. Chang, J. He, H. Wang, X. Zhou, F. Xiao, C. Gao, Classification of VLF/LF lightning signals using sensors and deep learning methods, *Sensors* 20 (4) (2020) <http://dx.doi.org/10.3390/s20041030>, URL <https://www.mdpi.com/1424-8220/20/4/1030>.
- [30] Y. Zhu, P. Bitzer, V. Rakov, Z. Ding, A machine-learning approach to classify cloud-to-ground and intracloud lightning, *Geophys. Res. Lett.* 48 (1) (2021) e2020GL091148, <http://dx.doi.org/10.1029/2020GL091148>, e2020GL091148, URL <https://agupubs.onlinelibrary.wiley.com/doi/abs/10.1029/2020GL091148>.
- [31] H. Kohlmann, W. Schulz, S. Pedeboy, Evaluation of EUCLID IC/CG classification performance based on ground-truth data, in: 2017 International Symposium on Lightning Protection, XIV SIPDA, 2017, pp. 35–41, <http://dx.doi.org/10.1109/SIPDA.2017.8116896>.
- [32] H. Heidler, Analytische blitzstromfunktion zur LEMP-berechnung, in: Proc. 18th Int. Conf. Lightning Protection, Munich, Germany, 1985, pp. 63–66.
- [33] C.A. Nucci, F. Rachidi, Experimental validation of a modification to the Transmission Line model for LEMP calculation, in: Proceedings 8th Symposium and Technical Exhibition on Electromagnetic Compatibility, Zurich, Switzerland, 1989, pp. 389–394.
- [34] V. Rakov, M. Uman, Review and evaluation of lightning return stroke models including some aspects of their application, *IEEE Trans. Electromagn. Compat.* 40 (4) (1998) 403–426, <http://dx.doi.org/10.1109/15.736202>.
- [35] M. Brignone, R. Procopio, M. Nicora, D. Mestriner, F. Rachidi, M. Rubinstein, A prony-based approach for accelerating the lightning electromagnetic fields computation above a perfectly conducting ground, *Electr. Power Syst. Res.* 210 (2022) 108125, <http://dx.doi.org/10.1016/j.epsr.2022.108125>.
- [36] V. Cooray, V. Scuka, Lightning-induced overvoltages in power lines: validity of various approximations made in overvoltage calculations, *IEEE Trans. Electromagn. Compat.* 40 (4) (1998) 355–363, <http://dx.doi.org/10.1109/15.736222>.
- [37] M. Rubinstein, An approximate formula for the calculation of the horizontal electric field from lightning at close, intermediate, and long range, *IEEE Trans. Electromagn. Compat.* 38 (3) (1996) 531–535, <http://dx.doi.org/10.1109/15.536087>.
- [38] M. Brignone, R. Procopio, M. Nicora, D. Mestriner, F. Rachidi, M. Rubinstein, A prony-based approach for accelerating the lightning electromagnetic fields computation: Effect of the soil finite conductivity, *Electr. Power Syst. Res.* 209 (2022) 108013, <http://dx.doi.org/10.1016/j.epsr.2022.108013>.
- [39] F. Rachidi, C. Nucci, M. Ianoz, C. Mazzetti, Influence of a lossy ground on lightning-induced voltages on overhead lines, *IEEE Trans. Electromagn. Compat.* 38 (3) (1996) 250–264.
- [40] A.K. Agrawal, H.J. Price, S.H. Gurbaxani, Transient response of multiconductor transmission lines excited by a nonuniform electromagnetic field, *IEEE Trans. Electromagn. Compat. EMC-22* (2) (1980) 119–129, <http://dx.doi.org/10.1109/TEMC.1980.303824>.
- [41] A. Borghetti, C. Nucci, M. Paolone, M. Bernardi, S. Malgarotti, I. Mastandrea, Influence of surge arresters on the statistical evaluation of lightning performance of distribution lines, in: 2004 International Conference on Probabilistic Methods Applied To Power Systems, 2004, pp. 776–781.
- [42] IEEE, Modeling of metal oxide surge arresters, *IEEE Trans. Power Deliv.* 7 (1) (1992) 302–309, <http://dx.doi.org/10.1109/61.108922>.
- [43] P. Pinceti, M. Giannettoni, A simplified model for zinc oxide surge arresters, *IEEE Trans. Power Deliv.* 14 (2) (1999) 393–398, <http://dx.doi.org/10.1109/61.754079>.
- [44] Tridelta-Meidenha, Metal oxide surge arrester with polymer cage-design Type series SBKC 3 to 144/SL-0, Tridelta Meidenha, Marie-Curie-Str. 3, 07629 Hermsdorf, Germany, 2022.
- [45] D. Mestriner, R.A. Ribeiro de Moura, R. Procopio, M.A. de Oliveira Schroeder, Impact of grounding modeling on lightning-induced voltages evaluation in distribution lines, *Appl. Sci.* 11 (7) (2021) <http://dx.doi.org/10.3390/app11072931>.
- [46] M. Brignone, D. Mestriner, R. Procopio, A. Piantini, F. Rachidi, On the stability of FDTD-based numerical codes to evaluate lightning-induced overvoltages in overhead transmission lines, *IEEE Trans. Electromagn. Compat.* 62 (1) (2020) 108–115, <http://dx.doi.org/10.1109/TEMC.2018.2890043>.
- [47] C. Alberto Nucci, A survey on Cigré and IEEE procedures for the estimation of the lightning performance of overhead transmission and distribution lines, in: 2010 Asia-Pacific International Symposium on Electromagnetic Compatibility, 2010, pp. 1124–1133, <http://dx.doi.org/10.1109/APEMC.2010.5475698>.
- [48] D. Mestriner, M. Brignone, R. Procopio, M. Nicora, E. Fiori, A. Piantini, F. Rachidi, An efficient methodology for the evaluation of the lightning performance of overhead lines, *IEEE Trans. Electromagn. Compat.* 63 (4) (2021) 1137–1145, <http://dx.doi.org/10.1109/TEMC.2021.3054427>.